Continental deformation in Asia from a combined GPS solution

E. Calais, L. Dong, M. Wang, Z. Shen, Mathilde Vergnolle

Continental Deformation in Asia from a Combined GPS Solution

E. Calais, L. Dong

Purdue University, Department of Earth and Atmospheric Sciences, West Lafayette, Indiana, USA

M. Wang

Institute of Earthquake Science, China Earthquake Administration, Beijing, China

Z. Shen

State Key Laboratory of Earthquake Dynamics, Institute of Geology, China Earthquake Administration, Beijing, China

M. Vergnolle

UMR 6526 CNRS Géosciences Azur, University of Nice, Valbonne, France. Now at UMR 5559 CNRS LGIT, Grenoble, France

After decades of research on continental tectonics, there is still no consensus on the mode of deformation of continents or on the forces that drive their deformation. In Asia the debate opposes edge-driven block models, requiring a strong lithosphere with strain localized on faults, to buoyancy-driven continuous models, requiring a viscous lithosphere with pervasive strain. Discriminating between these models requires continent-wide estimates of lithospheric strain rates. Previous efforts have relied on the resampling of heterogeneous geodetic and Quaternary faulting data sets using interpolation techniques. We present a new velocity field based on the rigorous combination of geodetic solutions with relatively homogeneous station spacing, avoiding technique-dependend biases inherent to interpolation methods. We find (1) unresolvable strain rates ($< 3 \times 10^9$/yr) over a large part of Asia, with current motions well-described by block or microplate rotations, and (2) internal strain, possibly continuous, limited to high-elevation areas.

1. Introduction

Geodetic measurements at sites located far enough away from active plate boundaries show that horizontal surface motions on most of our planet can be described by simple rotations of a limited number of rigid plates, as predicted by plate tectonics (*e.g.*, Argus and Heflin, 1995). In deforming continents such as Asia or the Western U.S., however, the ability of plate tectonic concepts to describe horizontal motions is still questioned (Thatcher, 2003). Indeed, observations and models of actively deforming continents such as Asia[1] have led to two opposing interpretations. For some, continental lithosphere deforms as a mosaic of rigid lithospheric blocks bounded by fast-slipping faults affecting the entire thickness of the lithosphere. In that view, deformation is solely driven by boundary forces due to the India-Eurasia collision (*e.g.*, Tapponnier et al., 1982; Peltzer and Tapponnier, 1988; Peltzer and Saucier, 1996). For others, deformation is

0094-8276/06/200XXXXXXXXXX$5.00

pervasive and continents can be treated as a continuously deforming viscous medium where faults play a minor role. In that view, deformation is driven for a large part by buoyancy forces resulting from crustal thickening in response to the India-Eurasia collision (*e.g.*, England and Houseman, 1986; Houseman and England, 1993).

In some instances, space geodetic studies have provided insight into this debate. For instance, GPS measurements show that the central part of the Altyn Tagh fault accumulates strain at a rate of 9 mm/yr (Bendick et al., 2000; Shen et al., 2001; Wallace et al., 2004), inconsistent with edge-driven block models that require slip rates at least a factor of two larger (Peltzer and Saucier, 1996). Geodetic measurements of the eastward velocity of south China at 8 to 10 mm/yr (*e.g.*, Wang et al., 2001) match block models and continuous deformation models equally well (Peltzer and Saucier, 1996; Molnar and Gipson, 1996) but proved wrong early models of extrusion that required at least 10-15 mm/yr of eastward motion of south China (Avouac and Tapponnier, 1993). At a continent-wide scale, Flesch et al. (2001), used an interpolated velocity field derived from heterogeneous GPS data and Quaternary fault slip rates to show that large parts of Asia undergo little internal deformation and that gravitational potential energy (GPE) contributes up to 50% to the force balance. England and Molnar (2005), using similar data but a different spatial resampling technique, argue that continuous deformation dominates.

Here, we combine geodetic solutions in Asia to produce a new velocity field with continent-wide coverage and relatively homogeneous station spacing, removing the need for spatial resampling, necessarily model-dependent. The kinematic analysis of this continent-wide data set shows unresolvable strain rates over a large part of Asia, while significant strain rates, possibly associated with continuous deformation, are limited to the high-elevation areas of the Himalaya, Tibet, Pamir-Tien Shan, and Western Mongolia.

2. GPS data

In order to obtain a geodetically consistent velocity field covering Asia, we combined three GPS solutions. The first one covers Mongolia, the Baikal rift zone, and the Russian Altay. It contains 110 survey sites, of which 64 have been observed at least 3 times from 1994 to 2004, and 3 continuous stations. The second one includes 83 stations in China measured between 1998 and 2005, of which 27 became continuous in 1999. The 56 other are measured annually, with 10 observation-days per site each year. The third one includes 41 sites in Southeast Asia with data spanning from 1991 to 2002 (Socquet et al., 2006). Although Socquet et al.'s (2006) original solution contains 191 sites, those located within active plate boundary zones in eastern Indonesia (Sulawesi, Timor, Irian Jaya) and the Philipines were not considered here.

For the first two data sets, we processed the pseudorange and phase GPS data single-day solutions, together with 16 reference stations of the International GPS Service (IGS) to serve as ties with the International Terrestrial Reference Frame (ITRF). Details on the data processing procedure can be found in Wang et al. (2003) and Calais et al. (2003) and are not repeated here. The resulting least squares adjustment vector and its corresponding variance-covariance matrix for station positions and orbital elements estimated for each independent daily solution were then combined with global Solution Independent Exchange format (SINEX) files from the IGS daily processing routinely done at Scripps Institution of Oceanography (http://sopac.ucsd.edu) into a single, unconstrained, global solution using the combination method described in Dong et al. (1998). The velocity error model includes a 2 mm/$\sqrt{yr}$ random walk component to account for colored noise in GPS uncertainties. We imposed the reference frame by minimizing the position and velocity deviations of 25 core IGS stations with respect to the ITRF2000 (Altamimi et al., 2002) while estimating an orientation and translation (and their rate-of-change) transformation (12 parameters). These 25 reference stations, globally distributed, were chosen for having velocity uncertainties less that 2 mm/yr on the horizontal and 5 mm/yr on the vertical components in the ITRF2000 definition. The post-fit fweighted root-mean-square (WRMS) of the reference frame stabilization is 2.0 mm in position and 0.6 mm/yr in velocity. We then combined the resulting solution with that of Socquet al. (2006) for Southeast Asia, by estimating a 7-parameter transformation (translation, rotation, and scale) based on 12 IGS stations common to the two solutions. The WRMS of the velocity differences at the common sites is 1.2 mm/yr.

We mapped the resulting velocities (in ITRF2000) into a Eurasia-fixed frame by minimizing velocities at 15 sites distributed across the Eurasian plate (YAKT, IRKT, KSTU, ARTU, ZWEN, GLSV, GRAZ, WSRT, POTS, WTZR, KOSG, CAGL, NRIL, NVSK, VILL), while propagating the variance of the ITRF2000-Eurasia angular velocity to the individual site velocities. These 15 reference sites are chosen to cover the entire stable part of the Eurasian plate and are located away from areas potentially affected by tectonic deformation or significant glacial isostatic adjustment effects (Calais et al., 2003). The resulting GPS velocity field describes horizontal surface motions at 188 sites in Asia with a precision ranging from 0.5 to 3.5 mmr/yr (Figure 1[2]). In the following, we discard from the intrepretation sites with velocity uncertainties larger than 1.5 mm/yr. These sites, mostly located in the Mongolia-Altay-Baikal area, are consistently campaign sites with less than 3 observations epochs.

3. Velocity field

The combined GPS velocity field (Figure 1) and velocity profiles (Figure 2) illustrate the known convergence between India and the Tarim basin, the eastward motion of Tibet and south China and the clockwise rotation of eastern Tibet around the eastern Himalayan syntaxis. Convergence between India and Eurasia occur at 38 mm/yr (from velocities at sites Bangalore and Hyderabad in southern India), consistent with GPS-derived plate motion parameters for India (Paul et al., 2001; Sella et al., 2002). The western velocity profile (Figure 2A) shows consistent NNE-directed azimuths with velocity magnitudes steadily decreasing northward, indicative of NNE-SSW shortening. About 20 mm/yr of the total shortening is accommodated in the Himalayas, as previously reported by Bilham et al. (1997), while the remaining 17 mm/yr are distributed from Tibet to the Siberian platform, mostly taken up in the Tien Shan (17 mm/yr in the west, decreasing eastward to less than 10 mm/yr).

On the central profile (Figure 2B), horizontal velocities show a more complex pattern, with about 20 mm/yr of shortening accommodated in the Hymalayas and Tibet, but no shortening north of the Qilin Shan. This NNE-SSW shortening is accompanied, in Tibet, by up to 17 mm/yr of ESE-ward motion. North of the Qilin Shan, across western Mongolia and all the way to the Baikal rift zone velocities are directed ESE-ward at 3 to 5 mm/yr.

On the eastern profile (Figure 2C), horizontal motions are mostly directed to the east or southeast, with a steady increase in magnitude from 0 to about 9 mm/yr from north to south across north and south China. This consistent pattern of east- to southeastward motions from eastern Mongolia, north China, and south China, is a striking feature of this velocity field and had not yet been documented at that scale.

To separate block rotations from distributed strain, we attempt to describe the horizontal velocity field in terms of rotations of non-deforming blocks or microplates. To do so, we use the trace of major active faults in Asia (Figure 1) to divide the velocity field into 6 subsets of sites, representing the following blocks: North China (or "Amurian plate" of Zonenshain and Zavostin, 1981), South China, Sunda (*e.g.*, Chamot-Rooke and Le Pichon, 1999; Bock et al., 2003), Tarim basin, Qaidam basin, and Central Tibet. In Tibet, we limit our analysis to two blocks, Qaidam and Central Tibet, bounded by the Altyn Tagh, Kunlun, and Jiali faults (Chen et al., 2004) because the low density of sites in our solution does not provide the resolution necessary to investigate kinematics at smaller spatial scales. Also, we omit GPS sites located within actively deforming structures in the Himalayas, the Tien Shan, western Mongolia (Altay and Gobi Altay), Eastern Tibet (Karakorum and Pamir), Western Tibet (Longmen Shan), and in the Ordos, possibly affected by non-secular deformation processes on these active tecctonic structures (*e.g.*, interseismic strain accumulation or postseismic deformation). For the same reason, we omit sites located within 500 km of the Andaman-Sumatra-Java subduction, where elastic loading effects are significant (Chamot-Rooke and Le Pichon, 1999). We then solve for block angular rotations with respect to Eurasia by inverting the model that relates horizontal site velocities to plate angular velocity. Table 1 shows the resulting angular rotations and corresponding statistics, while Figure 1 (bottom) shows residual velocities after subtracting the estimated rotations.

The fit to a block rotation is good for most site subsets, with reduced chi-squared close to unity, except for the Qaidam and Central Tibet subsets. The fit in Tibet is not improved by considering Qaidam and Central Tibet as a single block, consistent with previous reports of block motions and internal deformation from denser GPS measurements in Tibet (Chen et al., 2004). The fit to a rigid rotation is particularly good for South China, with a weighted velocity residual RMS of 0.4 mm/yr. For North China, the resulting angular velocity is consistent with a recent estimate by Apel et al. (2006), based on a similar dataset. It is significantly different from previous estimates from Kreemer et al. (2003), Sella et al. (2003), and Prawirodirdjo and Bock (2004), but those were constrained by 3 sites only. The rotation poles for North and South China are located in eastern Siberia and associated with a counter-clockwise rotation with respect to Eurasia. The linear gradient in eastward velocities from north to south on Profile C (Figure 2) and the lack of offset at the boundary between North and South China may suggest that they constitute a single plate. We tested the significance of the χ^2 decrease from a solution where North and South China are treated as a single block to a solution where they are treated as two separate blocks using an F-test (Stein and Gordon, 1984). The F-statistics, defined as $(\chi^2_{1plate} - \chi^2_{2plates}/3)/(\chi^2_{2plates}/72)$ is 2.3, implying that the χ^2 decrease is significant at the 92% level. The data is therefore better fit by a splitting North and South China into two separate plates, although not at a very high significance level.

Our rotation pole for Sunda is located southwest of Australia, with a clockwise rotation with respect to Eurasia. These parameters differ significantly from those of Chamot-Rooke and Le Pichon (1999), possibly because of different definition of the Eurasia frame. They also differ from those of Bock et al. (2003), but these authors considered Sunda and South China as a single block. Using a F-test, we find that the χ^2 decrease when splitting Sunda and South China compared to treating them as a single block is significant at the 99.9% confidence level, indicating that our data is fit significantly better by a two-plate model.

4. Strain distribution

The above analysis in terms of block rotations is limited by the a priori choice of block boundaries and site subsets. An alternative approach consists of calculating horizontal strain rates over the study area. To do so, we discretize the study area using a Delaunay triangulation and calculate, for each triangle, the strain rate tensor with its covariance matrix, its level of significance, the principal strain rates, and the second invariant of the strain rate tensor – or effective strain rate – given by $\dot{E} = \sqrt{(\dot{\epsilon}_{ij}\dot{\epsilon}_{ij})/2}$, where $\dot{\epsilon}_{ij}$ are the components of the strain rate tensor and summing over repeated subscripts applies.

The resulting maps (Figure 3) show that strain rates are significant at the 95% confidence in the Himalayas, Tibet, Pamir-Tien Shan, Altay and Gobi Altay, with principal compressional axis consistent with shortening perpendicular to these structures. Within Tibet, principal strains show a combination of NNE-SSW compression and WNW-ESE extension, consistent with previous results (Wang et al., 2001; Zhang et al., 2004) and geologic observations of widespread extension on NS-trending normal faults in Tibet (*e.g.*, **Armijo et al., 1986**; Yin et al., 1999; Kapp and Guynn, 2004). Strain rates are also significant in the Baikal rift zone and directly west and southwest of it in the Hovsgol, Darkhat, and Busingol grabens, with extensional maximum principal strain perpendicular to the major normal faults. Effective strain rates in all these regions are larger than 3×10^{-9}/yr and reach maximum values of 2-3×10^{-8}/yr in the Himalayas, Burma, and along the eastern edge of the Tibetan plateau.

Strain rates are not significant at the 95% confidence level in the rest of Asia (including the Tarim basin, central and eastern Mongolia, north and south China, and Sunda). These regions also show effective strain rates less than 3×10^{-9}/yr, which corresponds to the current precision level of the GPS data set (average triangle dimension $\sim$ 300 km, velocity precision $\sim$ 1 mm/yr). These regions of unresolvable strain rate, at the current precision of the GPS data, are consistent with the major blocks or microplates defined above. Strain rates in a significant part of Asia (about 60% of the area considered in this study) are therefore comparable to stable plate interiors (less than 3×10^{-9}/yr) and not resolvable at the current precision level of GPS measurements in Asia.

Our findings contrast with England and Molnar's

(2005) conclusion that continuous deformation dominates in Asia, while block-like motions are restricted to the Tarim basin and small portions of north and south China. The difference likely results from England and Molnar's modeling approach, which resamples heterogeneous GPS data sets and Quaternary fault slip rates over a coarse triangular grid with linear shape functions. Our results match Flesch et al.'s (2001) interpolated kinematic model better, which however does not fit the observed east to southeastward velocities in Mongolia and North China. However, we do find, like Flesch et al. (2001) and England and Molnar (2005), a radial pattern in principal compressional strain rate directions around Tibet aligned with gradients of gravitational potential energy, an argument used by England and Molnar (2005) to support the idea that buoyancy forces play a significant role in driving present-day deformation in Asia.

5. Conclusion

The debate on continental deformation in Asia opposes edge-driven block models, requiring a strong lithosphere with strain localized on faults, to buoyancy-driven continuous models, requiring a viscous lithosphere with pervasive strain. As shown here, block- or plate-like motions appear to provide an accurate kinematic description of surface deformation for most of Asia. Similar conclusions have been drawn at a smaller scale for Tibet (Thatcher, 2005) and the Western U.S. (*e.g.*, Meade and Hager, 2005). Although these results apparently favor block models, they do not rebut continuous deformation models, provided that significant lateral variations in lithospheric strength exist. This is supported by results from Flesch et al. (2001), who show that vertically averaged effective viscosity in Asia varies laterally by up to 3 orders of magnitude. The GPS velocity field presented here does not resolve, by itsef, the debate on continental deformation but provides new quantitative information to validate physical theories on driving forces.

Acknowledgments. We thank our collaborators in Russia (Institute of the Earth Crust, Irkutsk and Institute of Geology, Geophysics, and Mineralogy, Novosibirsk, Siberian Branch of the Russian Academy of Sciences), Kazakhstan (Institute for High Temperatures), Mongolia (Research Center for Astronomy and Geophysics), for their invaluable contribution to the collection and processing of the GPS data. We thank A. Socquet and C. Vigny for making their GPS results available in advance of publication. Insightful reviews by P. Molnar and an anonymous reviewer and discussions with L. Flesch significantly helped improve the manuscript. This work was funded by NSF under award EARXXXX, CNRS-INSU (*"Intérieur de la Terre" Program*).

Notes

1. Supplemental Material is available at ftp://ftp.agu.org/apend/gl/2006GL28433
2. See Supplemental materials

References

Altamimi, Z., P. Sillard, and C. Boucher, ITRF2000: A New Release of the International Terrestrial Reference Frame for Earth Science Applications, *J. Geophys. Res.*, 10.1029 / 2001JB000561, 2002.

Apel, E., R. Bürgmann, G. Steblov, N. Vasilenko, R.W. King, and A. Prytkov, Independent Active Microplate Tectonics of Northeast Asia from GPS Velocities and Block Modeling, *Geophys. Res. Letters*, in press, 2006.

Argus, D. and Heflin, M., Plate motion and crustal deformation estimated with geodetic data from the Global Positioning System, *Geophys. Res. Lett, 22*, 1973–1976, 1995.

Armijo, R., Tapponnier, P., Mercier, J.L., and Han, T.-L., Quaternary extension in southern Tibet: Field observations and tectonic implications, *J. Geophys. Res., 91*, 13,803-13,872, 1986.

Avouac, J.P., and P. Tapponnier, Kinematic model of deformation in central Asia, *Geophys. Res. Letters, 20*, 895-898, 1993.

Bendick, R., Bilham, R., Freymueller, J., Larson, K., and Yin, G. (2000). Geodetic evidence for a low slip rate in the Altyn Tagh fault system. *Nature, 404*, 69–72, 2000.

Bock, Y., L. Prawirodirdjo, J. F. Genrich, C. W. Stevens, R. McCaffrey, C. Subarya, S. S. O. Puntodewo, E. Calais, Microplate Tectonics of Indonesia from Global Positioning System Measurements, 1989-1994, *J. Geophys. Res.*, Vol. 108, No. B8, 2367, 10.1029/ 2001JB000324, 2003.

Calais, E., M. Vergnolle, V. Sankov, A. Lukhnev, A. Miroshnitchenko, S. Amarjargal, and J. Deverchère, GPS measurements of crustal deformation in the Baikal-Mongolia area (1994-2002): Implications for current kinematics of Asia, *J. Geophys. Res., 108*, doi:10.1029/ 2002JB002373, 2003.

Chamot-Rooke, N., and X. Le Pichon, GPS determined eastward Sundaland motion with respect to Eurasia confirmed by earthquakes slip vectors at Sunda and Philippine trenches, *Earth Planet. Sci. Lett., 173*, 439-455, 1999.

Chen, Q., J.T. Freymueller, Q. Wang, Z. Yang, C. Xu, and J. Liu, A deforming block model for the present-day tectonics of Tibet. *J. Geophys. Res.*, 109, B01403, doi:10,1029/2002JB002151, 2004.

Cobbold, P.R. and Davy, P., Indentation tectonics in nature and experiment. 2. Central Asia. *Bull. Geol. Inst. Uppsala, 14*, 143–162, 1988.

Dong, D., T.A. Herring, and R.W. King, Estimating Regional Deformation from a Combination of Space and Terrestrial Geodetic Data, *J. of Geodesy, 72*, 200-214, 1998.

England P., P. Molnar, Late Quaternary to decadal velocity fields in Asia. *J. Geophys. Res., 110*, B12401, doi:10.1029/2004JB003541, 2005.

England, P. and Houseman, G., Finite strain calculations of continental deformation, 2. Comparison with the India-Asia collision zone. *J. Geophys. Res., 91*, 3664–3676, 1986.

Flesch, L.M., Haines, A.J., and Holt, W.E., Dynamics of the India-Eurasia collision zone. *J. Geophys. Res., 106*, 16435–16460, 2001.

Houseman, G. and England, P., Crustal thickening versus lateral expulsion in the India-Asian continental collision. *J. Geophys. Res., 98*, 12233–12249, 1993.

Kapp, P., and J. Guynn, Indian punch rifts Tibet, *Geology, 32*, 993-996, doi: 10.1130/G20689.1, 2004.

Meade, B.J., and B.H. Hager, Block models of crustal deformation in southern California constrained by GPS measurements, *J. Geophys. Res., 110*, doi:10.1029/2004JB003209, 2005.

Paul, J., R. Bürgmann, V. K. Gaur, R. Bilham, K. M. Larson, M. B. Ananda, S. Jade, M. Mukal, T. S. Anupama, G. Satyal, and D. Kumar, The motion and active deformation of India, *Geophys. Res. Letters, 28*, 647–650, 2001.

Peltzer, G. and Saucier, F., Present-day kinematics of Asia derived from geological fault rates. *J. Geophys. Res., 101*, 27943–27956, 1996.

Peltzer, G. and Tapponnier, P., Formation and evolution of strike-slip faults, rifts, and basins during the India-Asia collision: An experimental approach. *J. Geophys. Res., 315*, 15085–15117, 1998.

Sella, G. F., T. H. Dixon and A. Mao, REVEL: A model for recent plate velocities from Space Geodesy, *J. Geophys. Res., 107*, 10.109 / 2000JB000033, 2002.

Shen, Z.K., Wang, M., Li, Y., Jackson, D.D., and Yin, A., Dong, D., and Fang, P., Crustal deformation along the Altyn Tagh fault system, western China, from GPS. *J. Geophys. Res., 106*, 30607–30621, 2001.

Socquet A., C. Vigny, N. Chamot-Rooke, W. Simons, C. Rangin, and B. Ambrosius, India and Sunda plates motion and deformation along their boundary in Myanmar determined by GPS, *J. Geophys. Res., 111*, B05406, doi:10.1029/2005JB003877, 2006.

Stein, S., and R.G. Gordon, Statiistical tests of additional plate boundaries from plate motion inversions, *Earth and Planetary Sci. Lett., 69*, 401–412, 1984.

Tapponnier, P., Peltzer, G., Le Dain, A.Y., Armijo, R., and Cobbold, P. Propagating extrusion tectonics in Asia: New insights from simple experiments with plasticine. *Geology, 10*, 611–616, 1982.

Thatcher, W., GPS constraints on the kinematics of continental deformation. *Int. Geol. Rev., 45*, 191–212, 2003.

Thatcher, W., Present-Day Microplate Tectonics of Tibet and its Relation to Rheological Stratification and Flow in the Lithosphere, *Eos Trans. AGU, 86(52)*, Fall Meet. Suppl., Abstract U51B-04, 2005.

Vilotte, J.P., Daignieres, M., and Madariaga, R., Numerical modeling of intraplate deformation: Simple mechanical models of continental collision. *J. Geophys. Res., 87*, 19709–19728, 1982.

Wang, Q., Zhang, P.Z., Freymueller, J.T., Bilham, R., Larson, K., Lai, Z., You, X., Niu, Z., Wu, J., Li, Y., Liu, J., Yang, Z., and Chen, Q., Present-Day Crustal Deformation in China Constrained by Global Positionning System Measurements. *Science, 294*, 574–577, 2001.

Wang, M., Z.K. Shen, Z. Niu, et al., Contemporary crustal deformation of Chinese continent and blocking motion model, *Science in China, 33(supp)*, 19-32, 2003.

Yin, A., Kapp, P.A., Murphy, M.A., Harrison, T.M., Grove, M., Ding, L., Deng, X., and Wu, C., Significant late Neogene east-west extension in northern Tibet, *Geology, 27*, 787-790, 1999.

Zhang, P., Z.-K Shen, M. Wang, et al., Continuous deformation of the Tibetan Plateau from global positioning system data, *Geology, 32*, 809-812, 2004.

E. Calais, L. Dong, Purdue University, EAS Department, West Lafayette, IN 47907, USA. (ecalais@purdue.edu)

M. Wang, Institute of Earthquake Science, China Earthquake Administration, 63 Fuxing Rd, Beijing 100036, China. (mwang@gps.gov.cn)

Z. Shen, State Key Laboratory of Earthquake Dynamics, Institute of Geology, China Earthquake Administration, P.O. Box 9803, Beijing 100029, China. (zshen@ies.ac.cn)

M. Vergnolle, Laboratoire de Géophysique Interne et Tectonophysique, Maison des Géosciences, BP 53, 38041 Grenoble Cedex 9, France (mathilde.vergnolle@obs.ujf-grenoble.fr)

Block	χ_r^2	dof	λ	ϕ	σ_{maj}	σ_{min}	θ	ang	WRMS
N. China	1.0	43	54.6	135.149	4.6	2.15	27.2	0.079±0.016	0.6
S. China	1.2	29	55.1	127.253	3.3	0.89	63.8	0.110±0.008	0.4
NS China	1.2	75	53.1	127.427	1.7	0.75	61.4	0.111±0.005	0.7
Tarim	1.6	9	-36.9	-79.7	1.6	0.7	25.7	0.438±0.036	0.7
Sunda	1.5	47	44.3	-73.3	16.9	2.5	86.5	0.062±0.011	1.2
Qaidam	9.1	3	-29.2	-76.5	1.5	0.4	60.6	0.570±0.063	2.5
C. Tibet	10.1	5	-22.5	-80.7	1.7	0.4	61.9	0.905±0.084	1.6

Table 1. Angular velocities. χ_r^2 is the chi-squared per degree of freedom (dof). λ and ϕ are the latitude and longitude, respectively, of the Euler pole describing the block rotation with respect to Eurasia (in decimal degrees). σ_{maj} and σ_{min} are the semi-major and semi-minor axes of the pole error ellipse in degrees. θ is the direction of the semi-major axis in degrees counterclockwise from East. Ang. is the rotation rate in degrees per Ma. WRMS is the weighted root mean square of residual velocities for each block.

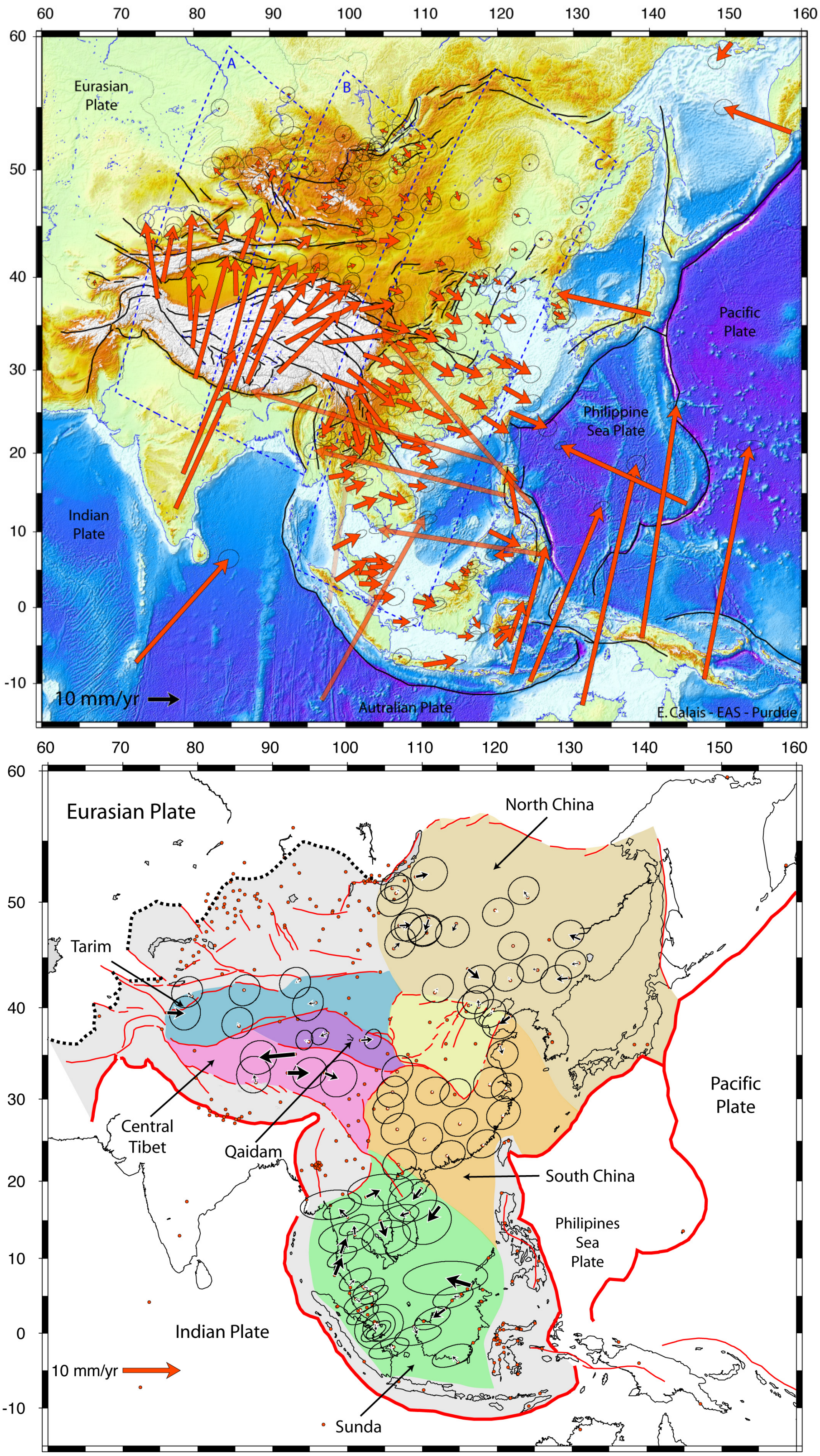

Figure 1. Top: Horizontal GPS velocities shown with respect to Eurasia. Large velocities at sites on adjacent plates are shown transparent for a sake of readability. The dashed boxes show the domains included in the 3 profiles (A, B, C) shown on Figure 2. Bottom: Residual velocities after subtracting ~~rigid~~ block rotations (see explanations in text). Dots show the location of all GPS sites. Major blocks used here are shown with color background. White areas were not included in the block analysis. Error ellipses are 95% confidence interval on both figures.

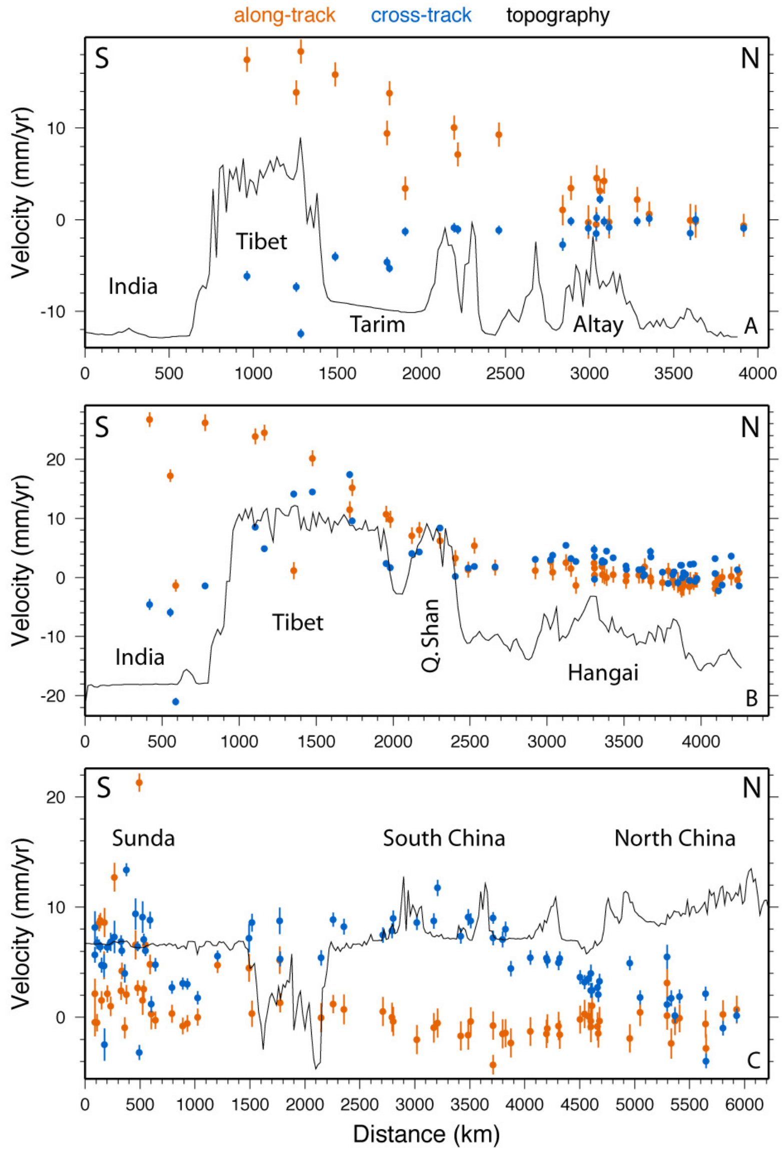

Figure 2. Velocity profiles: GPS velocity components projected into profile-parallel (along-track) and profile-perpendicular (cross-track) directions. The profile locations and sites included are shown on Figure 1 (top).

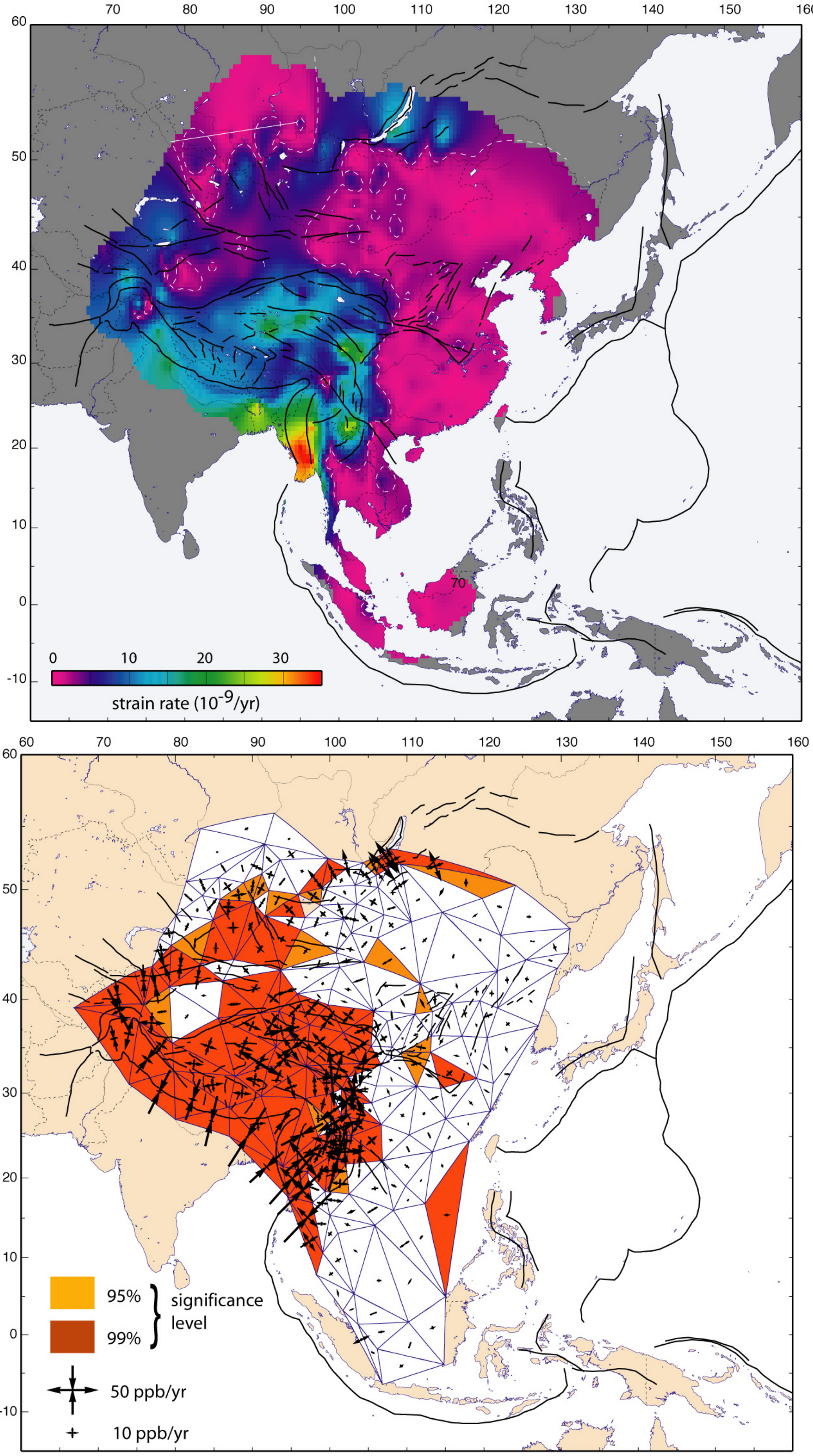

Figure 3. Top panel: Second invariant of the stain rate tensor calculated for a Delaunay triangulation (see bottom panel). The white dashed line shows the 3×10^{-9} yr-1 contour. Bottom panel: Delaunay triangulation of the GPS network shown on Figure 1 with principal axis of the strain rate tensor shown at the centroid of each triangle. Convergent arrows mean contractional strain, divergent arrows mean extensional strain. Yellow and orange triangles show domains where the strain rate tensor is significant at the 95% and 99% confidence level, respectively. White triangles indicate a sigificance level lower than 95%.